PAMOP Project: Petaflop Computations in Support of Experiments

B.M. McLaughlin, C.P. Ballance, M.S. Pindzola, S. Schippers, and A. Müller

Abstract Our computation effort is primarily concentrated in support of current and future measurements being carried out at various synchrotron radiation facilities around the globe and for charge transfer experiments. In our work we solve the Schrödinger or Dirac equation for the appropriate collision problem using the R-matrix or R-matrix with pseudo-states approach from first principles. The time dependent lattice (TDL) method is also used in our work on charge exchange. A brief summary of the methodology and ongoing developments implemented in the R-matrix suite of Breit-Pauli and Dirac-Atomic R-matrix codes (DARC) is presented. We illustrate vividly the sophistication level of large scale petaflop computations necessary to model accurately the spectra currently being measured at various synchrotron radiation facilities. The new Cray XC40 architecture installed at HLRS is playing a vital role in our computational effort.

1 Introduction

Our research efforts continue to focus on the development of computational methods to solve the Schrödinger and Dirac equations for atomic and molecular collision processes. Access to leadership-class computers such as the Cray XC40 at HLRS allows us to benchmark our theoretical solutions against dedicated collision experiments at synchrotron facilities such as the Advanced Light Source (ALS),

B.M. McLaughlin (✉)
Centre for Theoretical Atomic, Molecular and Optical Physics (CTAMOP), School of Mathematics & Physics, The David Bates Building, Queen's University, 7 College Park, Belfast BT7 1NN, UK
e-mail: b.mclaughlin@qub.ac.uk; bmclaughlin899@btinternet.com

C.P. Ballance • M.S. Pindzola
Department of Physics, 206 Allison Laboratory, Auburn University, Auburn, AL 36849, USA
e-mail: ballance@physics.auburn.edu; pindzola@physics.auburn.edu

S. Schippers • A. Müller
Institut für Atom-und Molekülphysik, Justers-Liebig-Universität Giessen, 35392 Giessen, Germany
e-mail: Stefan.E.Schippers@iamp.physik.uni-giessen.de; Alfred.Mueller@iamp.physik.uni-giessen.de

W.E. Nagel et al. (eds.), *High Performance Computing in Science and Engineering '15*, DOI 10.1007/978-3-319-24633-8_4

Astrid II, BESSY II, SOLEIL and PETRA III and to provide atomic and molecular data for ongoing research in laboratory and astrophysical plasma science. In order to have direct comparisons with experiment, semi-relativistic or fully relativistic computations, involving a large number of target-coupled states are required to achieve spectroscopic accuracy. These computations could not be even attempted without access to high performance computing (HPC) resources such as those available at leadership computational centers in Europe (HLRS) and the USA (NERSC, NICS and ORNL). We use the R-matrix and R-matrix with pseudo-states (RMPS) methods to solve the Schrödinger and Dirac equations for atomic and molecular collision processes.

Satellites such as *Chandra* and *XMM-Newton* are currently providing a wealth of X-ray spectra on many astronomical objects, but a serious lack of adequate atomic data, particularly in the *K*-shell energy range, impedes the interpretation of these spectra. With the impending launch of the Astro-H satellite in the spring of 2016, X-ray cross section data for a variety of atomic species of prominent astrophysical interest will be of paramount importance (Kallman 2015, private communication).

The motivation for our work is multi-fold; (a) Astrophysical Applications [11, 25, 28, 38, 41], (b) Fusion and plasma modelling [69, 70], (c) Fundamental interest and (d) Support of experimental measurements [6, 15] and Satellite observations. In the case of heavy atomic systems [39, 40], little atomic data exists and our work provides results for new frontiers on the application of the R-matrix; Breit-Pauli and DARC parallel suite of codes. Our highly efficient R-matrix codes are widely applicable to the support of present experiments being performed at synchrotron radiation facilities. Examples of our large scale petaflop computations for cross sections are presented below in order to illustrate the predictive nature of the methods employed as compared to experiment.

The main question asked of any method is, how do we deal with the many body problem? In our case we use first principle methods (ab initio) to solve our dynamical equations of motion. Ab initio methods provide highly accurate, reliable atomic and molecular data (using state-of-the-art techniques) for solving the Schrödinger and Dirac equation. The R-matrix non-perturbative method is used to model accurately a wide variety of atomic, molecular and optical processes such as; electron impact ionization (EII), electron impact excitation (EIE), single and double photoionization and inner-shell X-ray processes. The R-matrix method provides highly accurate cross sections and rates used as input for astrophysical modeling codes such as; CLOUDY, CHIANTI, AtomDB, XSTAR necessary for interpreting experiment/satellite observations of astrophysical objects and fusion and plasma modeling for JET and ITER.

2 Parallel R-Matrix Photoionization

The use of massively parallel architectures allows one to attempt calculations which previously could not have been addressed. This approach enables large scale relativistic calculations for trans-iron elements such as; Kr-ions, Xe-ions, Se-ions

[39, 40] and W-ions [2, 4]. It allows one to provide atomic data in the absence of experiment and takes advantage of the linear algebra libraries available on most architectures. We fill in our "*sea of ignorance*" i.e. provide data on atomic elements where none have previously existed. The present approach has the capability to cater for Hamiltonian matrices in excess of 400 K × 400 K. Examples are presented for both valence and inner-shell photoionization for systems of prime interest to astrophysics and for complex species necessary for plasma modeling in fusion tokamaks.

Further developments and refinements of the dipole codes benefit from similar modifications and developments made to the existing excitation R-matrix codes [40, 42, 44]. In this case all the eigenvectors from a pair of dipole allowed symmetries are required for bound-free dipole matrix formation. Every dipole matrix pair is carried out concurrently with weighted groups of processors assigned to an individual dipole. The method is applicable to photoionization, dielectronic recombination or radiation damped excitation and now reduces to the time taken for a single dipole formation. The method so far implemented on various parallel architectures has the capacity to cater for photoionization calculations involving ∼1500 levels. This dramatically improves (a) the residual ion structure, (b) ionization potential, (c) resonance structure and (d) can deal with in excess of 8000 close-coupled channels.

3 X-ray and Inner-Shell Processes

3.1 The Atomic Oxygen Iso-Nuclear Sequence

Theoretical studies on K-shell photoionization cross sections of neutral nitrogen and oxygen agree well with high resolution measurements made at the Advanced Light Source (ALS) radiation facility [45, 67]. Similarly cross section calculations along the atomic nitrogen iso-nuclear sequence compare favourably with high resolution measurements made at the SOLEIL synchrotron facility [1, 20, 21]. In fact the majority of the high-resolution experimental data from third generation light sources show excellent agreement with the state-of-the-art R-matrix method and with other modern theoretical approaches.

Here we concentrate on the atomic oxygen iso-nuclear sequence for the energy region in the vicinity of the K-shell. Absolute cross sections for the single and double K-shell photoionization of C-like (O^{2+}) and N-like (O^{+}) ions were measured in the 526 to 620 eV photon energy range by employing the ion-photon merged-beam technique at the SOLEIL synchrotron radiation facility [7]. High-resolution spectroscopy up to $E/\Delta E \approx 5300$ was achieved. Rich resonance structures observed in the experimental spectra (see Figs. 1 and 2) are analyzed and identified with the aid of R-matrix and MCDF methods. For these two atomic oxygen ions the strong $1s \rightarrow 2p$ and the weaker $1s \rightarrow np (n > 2)$ resonances observed are characterized [7]. A detailed comparison of the energies of the $1s \rightarrow 2p$ resonances

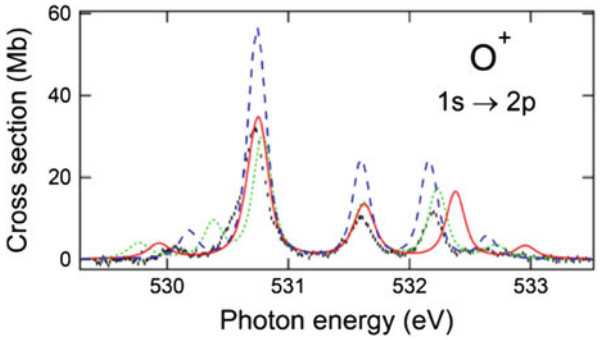

Fig. 1 Comparison in the *K*-shell region for the $1s \rightarrow 2p$ transitions in the O^+ ion for the single photoionization cross section measured with 100 meV band pass (*black points*) with the results of the MCDF (*blue dashed line*) and R-matrix RMPS (*red continuous line*) calculations with the previous optical potential R-matrix results of Garcia and co-workers [18] (*green dotted line*). The theoretical cross sections were reconstructed assuming relative populations of 40 % $^4S^o$, 40 % $^2D^o$ and 20 % $^2P^o$, then convolved with a 100 meV FWHM Gaussian profile. Note, the MCDF cross section calculation has been shifted by 1 eV towards higher energies [7]. The designation of these $1s \rightarrow 2p$ strong resonances (positions, widths and strengths) are presented in Table 1

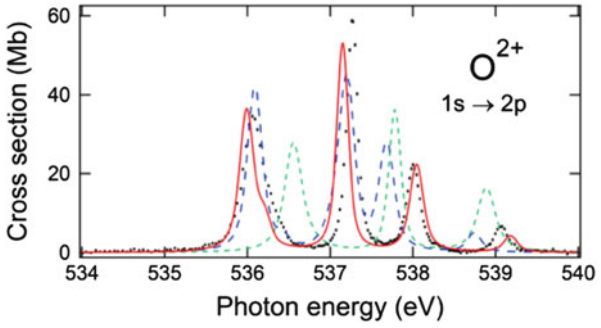

Fig. 2 Comparison in the *K*-shell region of the $1s \rightarrow 2p$ transitions in the O^{2+} ion for single photoionization cross section (*black points*) measured with 110 meV band pass with the results from MCDF (*blue dashed line*), R-matrix RMPS (*red continuous line*) calculations, and previous optical potential R-matrix results of Garcia and co-workers [18] (*green dotted line*). We assume relative populations of 80 % ^3P, 14 % ^1D, 4 % ^1S and 2 % $^5S^o$. The theoretical cross sections have been convolved by a 110 meV FWHM Gaussian profile [7]. The designation of these $1s \rightarrow 2p$ strong resonances (positions, widths and strengths) are given in Table 2

in the first members of the oxygen iso-nuclear sequence measured by synchrotron based experiments were made with the observations taken by the Chandra and XMM-Newton X-ray satellites [7].

The first experimental investigation on the atomic oxygen iso-nuclear sequence was performed for B-like atomic oxygen ions at the SOLEIL synchrotron radiation facility in Saint Aubin, France [43]. The results show suitable agreement for the photoionization cross sections produced by X-rays in the vicinity of the *K*-edge,

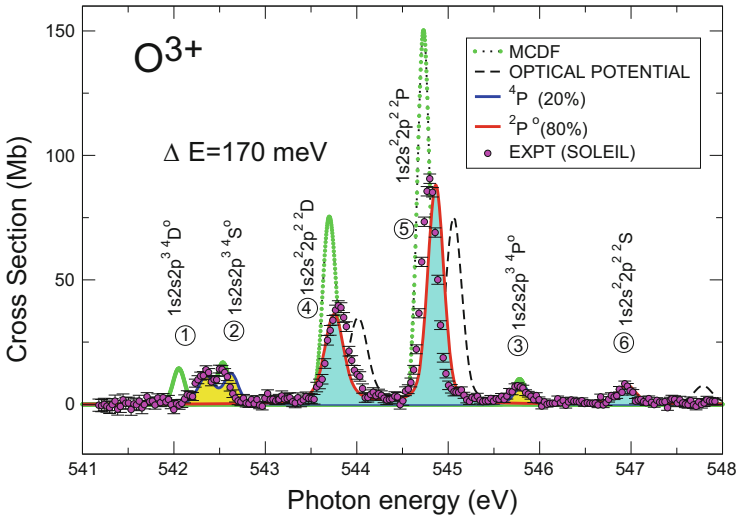

Fig. 3 Photoionization cross sections for O^{3+} ions measured with a 170 meV band pass in the region of 1s → 2p photo-excitations. *Solid points* (*magenta*), experimental cross sections. The error bars give the statistical uncertainty of the experimental data. The R-matrix (RMPS, *solid red line*, ground state, 80 % ^{2}P^o, metastable, *blue line* 20 % ^{4}P). *Dotted line* with *solid green circles* are MCDF calculations (80 % ^{2}P^o and 20 % ^{4}P). The optical potential R-matrix results (*dashed black line* 80 % ^{2}P^o) are from the results of Garcia and co-workers [18]. Theoretical work shown was convoluted with a Gaussian profile of 170 meV FWHM and a weighting of the ground and metastable states (see text for details) to simulate the measurements [43]

where strong n=2 inner-shell resonance states are observed. We note that atomic oxygen ions produced in the SOLEIL synchrotron radiation experiments are not purely in their ground state (see Figs. 1, 2, and 3). One therefore requires cross sections for the ground state and for metastable states present in the beam.

K-shell photoionization contributes to the ionization balance in a more complicated way than outer shell photoionization. In fact K-shell photoionization when followed by Auger decay couples three or more ionization stages instead of two in the usual equations of ionization equilibrium [1, 7, 21, 43].

The R-matrix with pseudo-states method (RMPS) was used to determine all the cross sections (in LS-coupling) with 390 levels of the respective atomic oxygen residual ions included in the close-coupling calculations. In the case of B-like (O^{3+}) oxygen ions, metastable states are present in the parent ion beam, theoretical PI cross-section calculations are required for both the $1s^2 2s^2 2p$ ^{2}P^o ground state and the $1s^2 2s 2p^2$ ^{4}P metastable states of the O^{3+} ion for a proper comparison with experiment. In order to simulate the experimental measurements cross sections have to be convoluted at the same resolution as experiment with an appropriate weighting of the initial states.

The scattering wavefunctions were generated by allowing three-electron promotions out of selected base configurations. Scattering calculations were performed with 20 continuum functions. In the case of the B-like atomic oxygen (O^{3+}) ion, $1s^2 2s^2 2p\ ^2P^o$ ground and the $1s^2 2s 2p^2\ ^4P$ metastable states the electron-ion collision problem was solved with a fine energy mesh of 2×10^{-7} Rydbergs ($\approx$2.72 μeV) to delineate all the resonance features in the PI cross sections.

Similarly, for C-like atomic oxygen (O^{2+}) ions, one requires cross sections for the $1s^2 2s^2 2p^2\ ^3P$ ground state, the $1s^2 2s^2 2p^2\ ^1D,^1S$ and $1s^2 2s 2p^3\ ^5S^o$ metastable states. Finally, for the case of N-like atomic oxygen (O^+), cross sections for ions in the initial $1s^2 2s^2 2p^3\ ^4S^o$ ground state and the $1s^2 2s^2 2 2p^3\ ^2D^o,^2P^o$ metastable states, need to be determined [7].

For O^{3+} ions for a direct comparison with the SOLEIL results, cross section calculations were convoluted with a Gaussian function of appropriate width and an admixture of 80 % ground and 20 % metastable states used to best simulate experiment. The peaks found in the theoretical photoionization cross section spectrum were fitted to Fano profiles for overlapping resonances as opposed to the energy derivative of the eigenphase sum method [1, 7, 21, 43]. In the case of O^{2+} ions to compare with the SOLEIL results we assume relative populations of 80 % ^3P, 14 % ^1D, 4 % ^1S and 2 % $^5S^o$ [7]. Finally for the case of O^+ ions an admixture of populations of 40 % $^4S^o$, 40 % $^2D^o$ and 20 % $^2P^o$ was used [7].

The results for all three atomic oxygen ions, O^+, O^{2+} and O^{3+}, are illustrated respectively in Figs. 1, 2 and 3 and in Tables 1 and 2.

The energies of the $1s \rightarrow 2p$ transitions for the first members of the atomic oxygen iso-nuclear series as determined from Chandra observations and synchrotron experiments are summarized in Table 3. While there is good agreement within the uncertainities in the case of O^+ ion, discrepancies observed for neutral oxygen [45] and the O^{3+} ion [43] (the Chandra observations are higher by 0.6 and 1.2 eV, respectively) are also present for the O^{2+} ion [7]. The SOLEIL measurements give results for the resonance lines lower by 0.5 eV than those deduced from the satellite spectra. We note that in the satellite observations, it is assumed that all the elements are in their gas phase. No account is taken of molecular or solid-state (grains) effects which can lead to shifts of 0.5–1.0 eV for the K resonance-line positions. We speculate this may be the difference between the synchrotron measurements and the satellite observations. Spectral resolution of the X-ray observations have a maximum resolving power of 1000 compared to 5300 in the synchrotron measurements. This is insufficient to resolve the three transitions from the ground term in O^{2+} and O^{3+} making uncertain the identification of the lines in the X-ray satellites spectra.

Table 1 N-like atomic oxygen 1s → 2p transitions, energies (eV), natural line widths Γ(meV) and oscillator strengths (f-values) for O^+ [$1s^2 2s^2 2p^3$ $^4S^o$,^{2} D^o,^{2} P^o → $1s2s^2 2p^4$ ^4P,^{2} D,^{2} P,^{2} S] lines are presented

Transition $^{2S_i+1}L_i$ ↘ $^{2S_f+1}L_f$	Energy (eV) Merged beam[a]	Energy (eV) Satellite	Energy (eV) R-matrix	Energy (eV) MCDF	Γ (meV) Expt[a]	Γ (meV) R-matrix	f-value Expt[a]	f-value Theory
$^2P^o$ —^{2} D	530.054 ± 0.028		529.936[g]	529.179[i]	86 ± 60	159[g]	0.039 ± 0.006	0.049[g]
			529.768[h]	529.930[b]		162[h]		0.048[h]
(line 1)			531.096[j]			134[j]		0.050[j]
								0.056[l]
$^2P^o$ —^{2} P	530.522 ± 0.028		530.687[g]	529.738[i]		125[g]	0.036 ± 0.005	0.093[g]
			530.381[h]	530.240[b]		120[h]		0.097[h]
(line 2)			531.441[j]			103[j]		0.098[j]
								0.124[l]
$^4S^o$ —^{4} P	530.720 ± 0.180[a]	530.96 ± 0.070[c]	530.764[g]	529.746[i]	158 ± 20	134[g]	0.216 ± 0.032	0.172[g]
	531.000 ± 0.500[b]	531.03 ± 0.100[d]	530.789[h]	531.640[b]		129[h]	0.192[d]	0.177[h]
(line 3)		530.97 ± 0.030[e]	533.132[j]			112[j]		0.184[i]
		530.80 ± 0.050[f]	532.093[l]					0.167[j]
		530.90 ± 0.300[k]						0.244[l]
$^2D^o$ —^{2} D	531.579 ± 0.023		531.627[g]	530.602[i]	159 ± 30	163[g]	0.063 ± 0.009	0.088[g]
			531.623[h]	532.310[b]		160[h]		0.091[h]
(line 4)			532.841[j]			134[j]		0.086[j]
								0.123[l]
$^2D^o$ —^{2} P	532.190 ± 0.023		532.378[g]	531.162[i]	170 ± 20	126[g]	0.044 ± 0.007	0.094[g]
			532.230[h]	532.620[b]		121[h]		0.095[h]

(continued)

Table 1 (continued)

Transition $^{2S_i+1}L_i$ ↘ $^{2S_f+1}L_f$	Energy (eV) Merged beam[a]	Energy (eV) Satellite	Energy (eV) R-matrix	Energy (eV) MCDF	Γ (meV) Expt[a]	Γ (meV) R-matrix	f-value Expt[a]	f-value Theory
(line 5)			533.185[j]			103[j]		0.088[j]
								0.126[l]
^{2}P^o −^{2} S	532.641 ± 0.044		532.956[g]	531.641[i]	430 ± 200	154[g]	0.067 ± 0.010	0.040[g]
			532.712[h]	534.050[b]		151[h]		0.040[h]
(line 6)			533.956[j]			128[j]		0.038[j]
								0.056[l]

The SOLEIL experimental values are compared to previous measurements and to results from MCDF and R-matrix calculations, in addition to previous theoretical work

[a]SOLEIL measurements [7]
[b]Spring-8 measurements [30]
[c]Chandra observations [27]
[d]Chandra observations [78]
[e]Chandra observations [36]
[f]Chandra observations [19]
[g]R-matrix with pseudostates [7]
[h]R-matrix Optical-potential [18]
[i]R-matrix [65]
[j]R-matrix [79]
[k]XMM-Newton observations [68]
[l]MCDF [7]

Table 2 C-like atomic oxygen 1s → 2p transitions, energies (eV), natural line widths Γ (meV) and oscillator strengths (f-values) for $O^{2+}[1s^2 2s^2 2p^2\ ^3P,^1D,^1S \rightarrow 1s2s^2 2p^3\ ^3P^o,^3D^o,^3S^o,^1D^o,^1P^o,^1S^o]$ and $O^{2+}[1s^2 2s2p^3\ ^5S^o \rightarrow 1s2s2p^4\ ^5P]$ lines are presented

Transition $^{2S_i+1}L_i \searrow {}^{2S_f+1}L_f$	Energy (eV) Merged beam	Energy (eV) Satellite	Energy (eV) R-matrix	Energy (eV) MCDF	Γ (meV) Expt	Γ (meV) Theory	f-value Expt[a]	f-value Theory
$^3P - {}^3D^o$	536.082 ± 0.023[a]	536.635 ± 0.116[c]	535.992[m]	536.090[l]	135 ± 8[a]	146[m]	0.098 ± 0.015	0.117[m]
			540.000[f]	531.836[k]		132[f]		0.119[g]
(line 1)			537.200[g]			128[h]		0.111[i]
			537.976[h]			143[i]		0.137[l]
			535.286[i]			207[j]		
			536.559[j]			186[k]		
$^1S - {}^1P^o$	536.254 ± 0.029[a]		536.190[m]	536.422[l]	163 ± 26[a]	134[m]		0.291[m]
			537.947[h]	538.596[k]		112[h]		0.335[l]
(line 2)						153[k]		
$^5S^o - {}^5P$			536.235[m]	536.997[l]		72[m]		0.203[m]
			534.000[f]	539.315[k]		87[f]		0.232[l]
			538.243[h]			68[h]		
						186[i]		
$^1D - {}^1D^o$			537.128[m]	537.138[l]		140[m]		0.216[m]
			548.000[f]	535.878[k]		118[f]		0.251[l]
			538.924[h]			116[h]		
						153[k]		
$^3P - {}^3S^o$	537.269 ± 0.180[a]	537.800 ± 0.020[c]	537.156[m]	537.229[l]	102 ± 7[a]	72[m]	0.145 ± 0.022	0.097[m]
	537.408 ± 0.093[b]	536.000 ± 0.100[d]	540.000[f]	533.664[k]		58[f]		0.102[g]
(line 3)		537.950 ± 0.180[e]	538.600[g]			56[h]		0.099[i]
			536.496[h]			61[i]		0.105[l]
			537.784			106[j]		
						107[k]		

(continued)

Table 2 (continued)

Transition $^{2S_i+1}L_i$ ↘ $^{2S_f+1}L_f$	Energy (eV) Merged beam	Energy (eV) Satellite	Energy (eV) R-matrix	Energy (eV) MCDF	Γ (meV) Expt	Γ (meV) Theory	f-value Expt[a]	f-value Theory
^{3}P $-^3$ P^o	538.007 ± 0.022		538.046[m]	537.681[l]	174 ± 6[a]	139[m]	0.078 ± 0.012	0.070[m]
			541.000[f]	533.970[k]		110[f]		0.067[g]
(line 4)			540.700[g]			128[h]		0.080[i]
			540.195[h]			137[i]		0.092[l]
			537.350[i]			213[j]		
			538.888[j]			186[k]		
^{1}D $-^1$ P^o	539.068 ± 0.004		539.181[m]	538.744[l]	103 ± 17[a]	134[m]	0.093 ± 0.014	0.072[m]
			545.000[f]	537.979[k]		111[f]		0.087[l]
(line 5)			541.138[g]			110[h]		
						153[k]		

The SOLEIL experimental values are compared to previous measurements and to results from MCDF and R-matrix calculations, in addition to previous theoretical work

[a]SOLEIL measurements [7]
[b]EBIT measurements [23]
[c]Chandra observations [19]
[d]XMM-Newton observations [68]
[e]Chandra observations [36]
[f]R-matrix [64]
[g]R-matrix [65]
[h]R-matrix Optical-potential [80]
[i]R-matrix [59]
[j]R-matrix [18]
[k]MCDF [9]
[l]MCDF [7]
[m]R-matrix with pseudostates [7]

Table 3 Comparison of the energy (in eV) of the 1s → 2p lines for the first members of the atomic oxygen iso-nuclear sequence in their ground state determined from the Chandra satellite observations [19, 36] and synchrotron radiation (SR) based experiments [7, 43, 45]

Element		Gatuzz and co-workers [19]	Liao and co-workers [36]	Synchrotron Experiments
O		527.548 ± 0.022	527.397 ± 0.013	526.790 ± 0.040[a]
O^{+}		530.800 ± 0.045	530.966 ± 0.025	530.720 ± 0.180[b]
O^{2+}	^{3}D	536.635 ± 0.116		536.082 ± 0.203[b]
	^{3}S	537.799 ± 0.023	537.942 ± 0.018	537.269 ± 0.180[b]
	^{3}P			538.007 ± 0.202[b]
O^{3+}	^{2}D			543.823 ± 0.213[c]
	^{2}P		546.263 ± 0.263	545.014 ± 0.181[c]
	^{2}S			547.128 ± 0.128[c]

The uncertainty in the absolute energy are included for completeness
[a]ALS, Stolte and co-workers [45]
[b]SOLEIL, Bizau and co-workers [7]
[c]SOLEIL, Bizau and co-workers, after recalibration [7, 43]

4 Valence Shell Photoionization

4.1 Tungsten (W) Atoms and Ions

Tungsten presently receives substantial scientific interest because of its importance in nuclear-fusion research. Due to its high thermal conductivity, its high melting point, and its resistance to sputtering and erosion tungsten is the favoured material for the wall regions of highest particle and heat load in a fusion reactor vessel [57]. Inevitably, tungsten atoms are released from the walls and enter the plasma. With their high atomic number, Z=74, they do not become fully stripped of electrons and therefore radiate copiously, so that the tolerable fraction of tungsten impurity in the plasma is at most 2×10^{-5} [56]. Understanding and controlling tungsten in a plasma requires detailed knowledge about its collisional and spectroscopic properties. Although not directly relevant to fusion, photoionization of tungsten atoms and ions is interesting because it can provide details about spectroscopic aspects and, as time-reversed photorecombination, provides access to the understanding of one of the most important atomic collision processes in a fusion plasma, electron-ion recombination. R-matrix theory is a tool to obtain information about electron-ion and photon-ion interactions in general. Electron-impact ionization and recombination of tungsten ions have been studied experimentally [35, 48, 66, 71, 74, 75] while there are no detailed measurements on electron-impact excitation of tungsten atoms in any charge state. Thus, the present study on photoionization of these complex systems and comparison of the experimental data with R-matrix calculations provides benchmarks and guidance for future theoretical work on electron-impact excitation.

4.2 Neutral Tungsten

Photoabsorption by neutral tungsten atoms in the gas phase has been studied experimentally by Costello et al. employing the dual-laser-plasma technique [10]. A few years later the production of W^+ and W^{2+} photo-ions from tungsten vapor was observed by Sladeczek et al. [73]. However, no experimental data have been available in the literature for tungsten ions prior to the present project. Direct photoionization of W^{q+} ions is included in the calculations by Trzhaskovskaya et al. [76] as time-reversed radiative recombination but is expected to be only a small contribution to the total photoionization cross section. Theoretical work using many-body perturbation theory (MBPT) has been carried out by Boyle et al. [8] for photoionization of neutral tungsten atoms. Theoretical treatment of photoabsorption using a relativistic Hartree-Fock (RHF) approach was reported by Sladeczek et al. [73] in conjunction with their experiments. Ballance and McLaughlin very recently performed detailed large-scale R-matrix calculations for the neutral tungsten atom [3] using the Dirac-Coulomb R-matrix method as implemented in the DARC codes [13], which the reader should consult for explicit details.

Here large-scale theoretical results are presented for photoionization of neutral atomic tungsten (W) in the photon region from threshold to 100 eV. The theoretical results were obtained from a Dirac-Coulomb R-matrix approach [15, 22, 60]. Neutral tungsten has respectively, the following ground state configurations and associated metastable levels, $5p^6 5d^4 6s^2\ {}^5\mathrm{D_J}$, where J=0, 1, 2, 3 and 4. Our DARC calculations are compared with the limited available experimental data (which is not absolute). In the absence of very detailed electron-impact excitation (EIE) experiments for Tungsten, the current photoionization measurements theory provide a road-map for future complimentary EIE calculations.

The calculations used a model that included 645-levels arising from the eight configurations of the W^+ residual ion: namely the $4p^6 4d^{10} 4f^{14} 5s^2 5p^6 5d^4 6s$, $4p^6 4d^{10} 4f^{14} 5s^2 5p^6 5d^3 6s^2$, $4p^6 4d^{10} 4f^{14} 5s^2 5p^5 5d^4 6s^2$, $4p^6 4d^{10} 4f^{14} 5s 5p^6 5d^4 6s^2$, we opened the $4f$-shell $4p^6 4d^{10} 4f^{13} 5s^2 5p^6 5d^4 6s^2$, $4p^6 4d^{10} 4f^{14} 5s^2 5p^6 5d^5$, the $4d$-shell $4p^6 4d^9 4f^{14} 5s^2 5p^6 5d^4 6s^2$ and finally the $4p$-shell $4p^5 4d^{10} 4f^{14} 5s^2 5p^6 5d^4 6s^2$.

For the ground and metastable initial states, of neutral W studied here, the outer region electron-ion collision problem was solved (in the resonance region below and between all thresholds) using a suitably chosen fine energy mesh of 1.2×10^{-4} Rydbergs ($\approx$1.6 meV) to resolve any resonance structure in the appropriate photoionization cross sections. The *jj*-coupled Hamiltonian diagonal matrices were adjusted so that the theoretical term energies matched the recommended experimental values of NIST [29].

In Fig. 4, we compare the ground term statistically averaged PI cross section result with the experiments of Costello and co-workers [10] and those of Haensel and co-workers [24]. At 35 eV, the dual laser experiment exhibits the onset of 4f ionization at approximately 3–4 eV before both the theoretical values of the MBPT [8] and the present DARC PI cross section calculations, however still within the

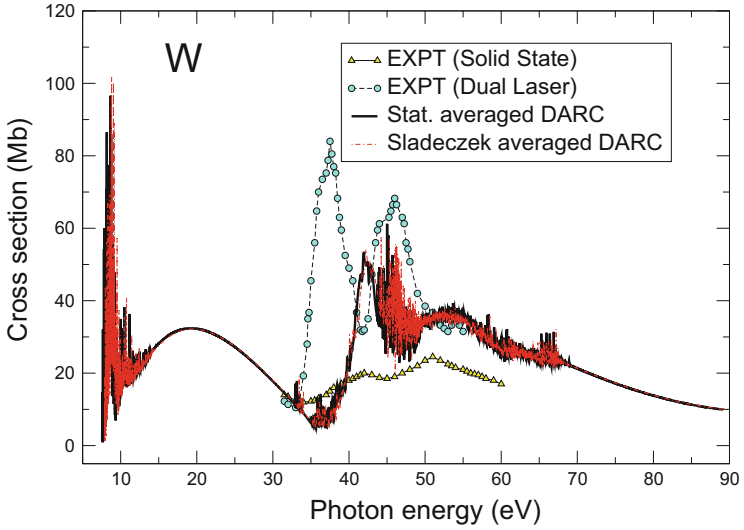

Fig. 4 Single photoionization of neutral W over the photon energy range 8–100 eV, comparing weighted averaged theoretical calculations with two different experiments. The DARC results (645-levels approximation, *solid black line*), are the statistical average of the five levels associated the ^{5}D term ground state. The (*dashed red-line*) is the weighted DARC results of the lowest six levels, employing the mixing coefficients reported by Sladeczek and co-workers [73]. *Solid circles* with *dashed line* are the dual-laser experimental results of Costello and co-workers [10] and the *solid triangles* are the results from the experimental work of Haensel and co-workers [24]. The statistically averaged DARC PI cross sections were Gaussian convolved at a FWHM of 250 meV

range of the other higher levels of the $6s^2$ configuration as reported in the NIST energy level table. This suggests that the metastable component of the experiment of Costello and co-workers [10] may include some of these higher levels. The Haensel experiment [24], from a solid-state target does not exhibit the strong 4f-5d, 5p-5d resonance structure to the same extent compared to all presented theories and the dual-laser experiment. The Sladeczek experiment [73] does not provide absolute values either, but in terms of a relative minimum to maximum ratio of the measurement is comparable to the Haensel and co-workers [24] experimental result. Sladeczek and co-workers [73] however report a relativistic Hartree-Fock calculation which is a mixture of the first six levels of neutral tungsten. We have employed these same six mixing coefficients with our present DARC PI cross section calculations, represented by the dashed-line in Fig. 4. Not surprisingly, as the individual PI cross sections are remarkably similar, (shifted slightly only by energy differences in the target), it provides a result in close prediction to the statistically averaged DARC result.

4.3 Singly Ionized Tungsten

For comparison with the measurements made at the ALS, state-of-the-art theoretical methods using highly correlated wavefunctions were applied that include relativistic effects [15, 22, 60]. An efficient parallel version [2, 4] of the DARC [13, 58, 77] suite of codes was applied which has been developed [16, 39, 40] to address electron and photon interactions with atomic systems providing for hundreds of levels and thousands of scattering channels. These codes are presently running on a variety of parallel high performance computing architectures world wide [42, 44]. Recently, DARC calculations on photoionization of trans-Fe elements were carried out for Se^+, Kr^+, Xe^+, and Xe^{7+} ions showing suitable agreement with high resolution ALS measurements [26, 39, 40, 49, 54].

For the Ta-like W^+ ion the present study is the first investigation on photoionization of tungsten ions and addresses singly charged W^+. Preliminary reports on our ongoing tungsten photoionization project have been presented at various conferences [51, 52, 55]. Müller and co-workers have recently made detailed measurements on the photoionization cross sections for singly ionized tungsten and compared them with large-scale DARC calculations [53] which are briefly summarised below.

First, we note that the ground level of the Ta-like W^+ ion is $5p^6 5d^4(^5D)6s\ ^6D_{1/2}$ with an ionization potential of (16.37 ± 0.15) eV [29]. One must assume that along with the $^6D_{1/2}$ ground level, the excited ground-configuration fine-structure levels ^6D_J with J=3/2, 5/2, 7/2 and 9/2 at excitation energies below 0.8 eV [29], respectively, are also populated in an ion source that produces W^+ by electron-impact ionization of neutral tungsten. Also the lowest levels of the first excited $5d^5$ and $5d^3 6s^2$ configurations have excitation energies below 2 eV and are likely populated in the ion-source plasma. The energetically lowest configurations $5p^6 5d^4 6s$, $5d^5$ and $5d^3 6s^2$ all have even parity and, hence, all the 118 excited levels within these configurations are long-lived because electric dipole transitions between any of these levels are forbidden. Any strong signal in the experimental photoionization spectrum below the threshold of (16.37 ± 0.15) eV would indicate the presence of metastable excited states in the parent ion beam, most likely within the $5p^6 5d^4(^5D)6s\ ^6D$, $5p^6 5d^5\ ^6S$ and $5p^6 5d^3 6s^2\ ^4F$ terms.

A part of the experimental and theoretical results is shown in Figs. 6 and 7. The direct and resonant photoionization processes occurring in the present energy range up to 245 eV for the interaction of a single photon with the ground-state and the lowest metastable configurations of the Ta-like tungsten ion comprise removal or excitation of either a $4f$, $5s$, $5p$, $5d$ or a $6s$ electron. For the theoretical description of W^+ photoionization suitable target wave functions have to be constructed that allow for promotions of electrons from these subshells to all contributing excited states. This is challenging for a low-charge ion such as W^+ but becomes simpler for the ions in higher charge states due to the increased effect of the Coulomb charge of the target and the slight reduction in the R-matrix box size.

Theory predicts narrow resonances at energies up to about 18 eV. Although the step width is too coarse in the experiment there is clear indication of rapid oscillations in the cross section at low photon energies. A relatively smooth energy dependence of the cross section follows at increasing photon energies. The experimental cross section goes over a very broad maximum while theory predicts a monotonically decreasing cross section. Around 35 eV the experimental result shows some structure and also narrow resonances again. The only channel calculated to provide significant amounts of resonance structure in this energy region is that for the ^{6}D term. This is further evidence of a substantial fraction of ions in their lowest-energy term present in the experiment (Fig. 5).

All calculations show the rapid increase of the cross section at photon energies above 35 eV that also characterizes the experimental result. The cross section maximum reached in each of the calculations is in close proximity of the experimental maximum. In the energy range 40 to 55 eV the details of the experimental cross section structure are not closely reproduced by the calculations or a reasonable combination of contributions from the investigated terms. These differences in the details are ascribed to the still very limited basis set of the calculations which was chosen to keep the computational effort manageable.

Beyond 55 eV the experimental cross section drops off rapidly. A similarly rapid decrease is only seen in the calculations for the ^{6}D term. The bump at about 60 eV in the experimental cross section is also seen in the theoretical data for the ^{6}S and ^{4}F terms. At energies beyond 70 eV theory overestimates the experimental single ionization cross section. Parts of the calculated ionization contributions may in fact end up in multiple-ionization channels after relaxation of the photoionized intermediate state formed by the removal of a single electron from W^+.

In energy ranges where narrow resonances could be observed, additional energy scans of the cross section were measured at 50 meV resolution. The most prominent occurrence of narrow features is in the energy range between about 30 and 36 eV. The top panel of Fig. 6 shows energy-scan results normalized to the absolute cross sections. Detailed resonance structure can be seen with the strongest peak feature occurring at about 35.5 eV just before the steep rise in the cross section due to the opening of the 4*f* subshell. The associated energy ranges of features in the theoretical cross sections are shown in the three lower panels. The energy axes of the calculated data were shifted in order to match certain features in the experimental cross section. It was felt that the experimental peak at 35.5 eV might correspond to the broad resonance structures in the ^{6}D and ^{6}S calculations occurring just below the steep rise in the cross section. Therefore, the theoretical energy scales were adjusted by -3.3 and -2.5 eV, respectively. In the ^{4}F calculations no corresponding peak could be found. The energy axis of the ^{4}F spectrum was shifted by -2.1 eV to match the steep onset of the 4*f* contribution to the cross section. Again it is the calculation for the ^{6}D initial term of W^+ ions that matches best with the experiment although the fine details of the measurements are not reproduced by theory.

Experimental and theoretical photoionization cross sections for W^+ ions are presented. The experimental cross sections were measured on an absolute scale

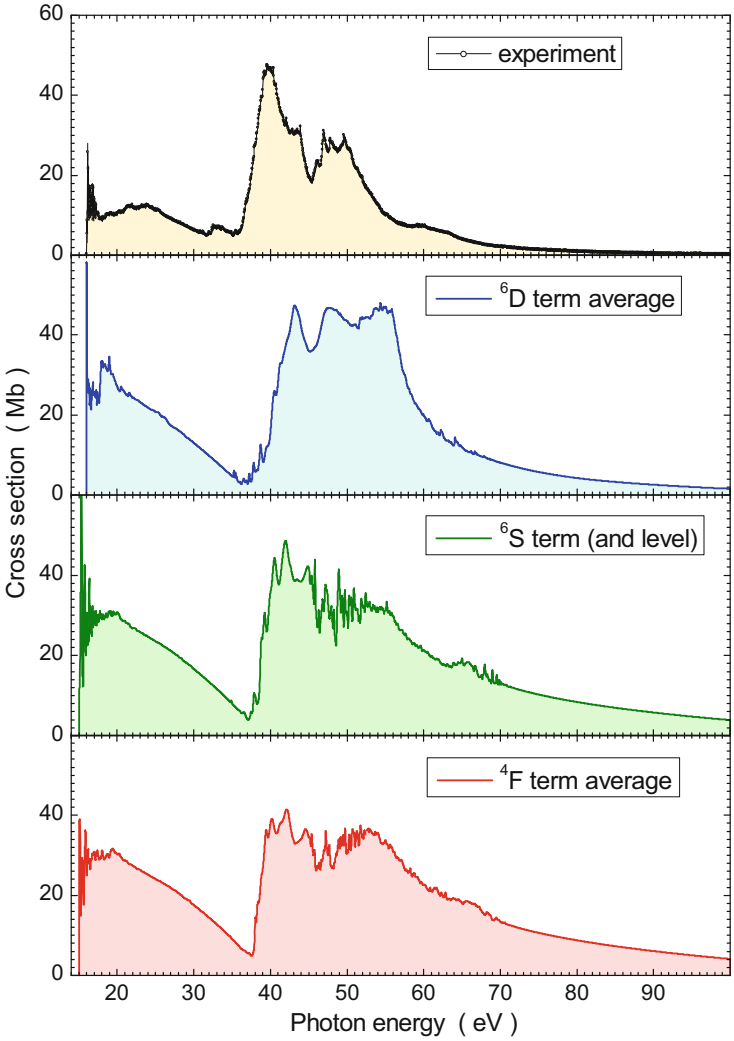

Fig. 5 Comparison of experimental and term-averaged theoretical photoionization cross sections of W^+ ions at 100 meV energy resolution. The three *lower panels* show the theoretical results obtained from 573-level DARC calculations for photoionization from the energetically lowest terms $5d^4 6s\ ^6$D, $5d^5\ ^6$S and $5d^3 6s^2\ ^4$F, respectively

employing the photon-ion merged-beam facility at the Advanced Light Source. The comparison of the measured and calculated results is complicated by the possible presence of long-lived excited states in the parent ion beams used for the experiments. More detailed modeling of the experimental data by theory would require calculations for at least all the 119 levels in the lowest configurations of the W^+ ion which is presently beyond the availability of computer resources. There

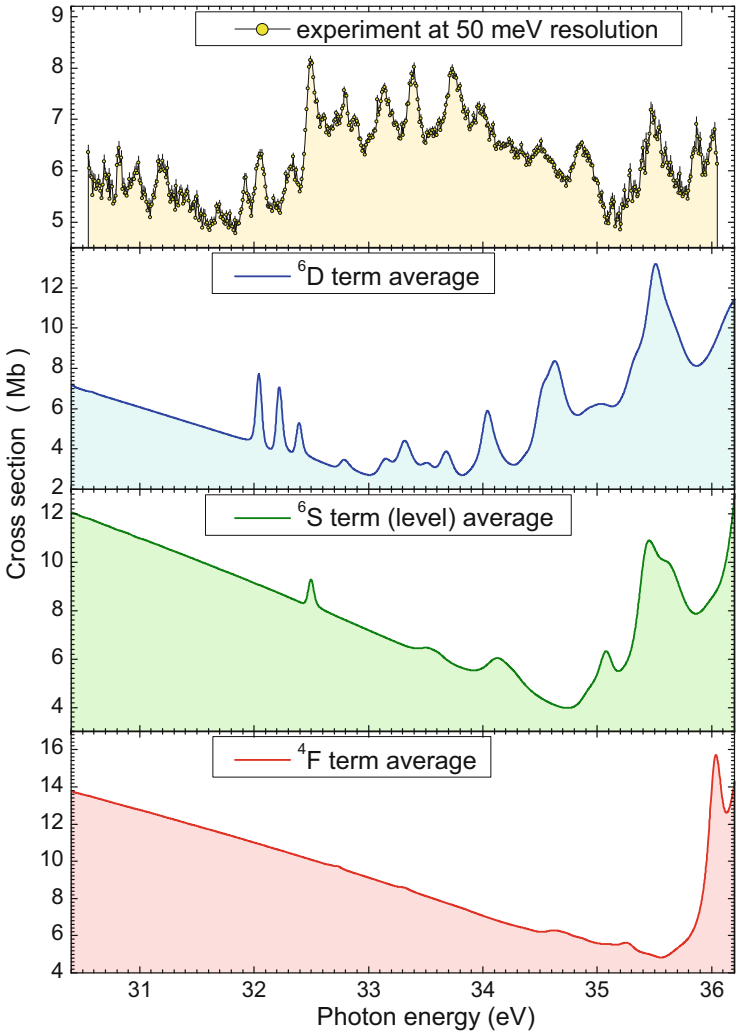

Fig. 6 Comparison of experimental and term-averaged theoretical photoionization cross sections of W^+ ions at 50 meV energy resolution in an energy range where narrow resonances occur in the cross section. The three *lower panels* show the theoretical results obtained from 573-level DARC calculations for the energetically lowest terms $5d^4 6s\ ^6$D, $5d^5\ ^6$S and $5d^3 6s^2\ ^4$F, respectively. The theoretical spectra are shifted in energy by −3.2, −2.5 and −2.1 eV, respectively. For more details see text

are indications, though, in the measured cross section that most of the parent ions were in the ground-state ^{6}D term. Given the existing limitations and considering the complexity of Ta-like tungsten with its open 5*d* subshell, one can conclude that the main features of the experimental results are reasonably well reproduced by the theoretical calculations. This result for a complex singly charged ion is encour-

aging for applying a similar theoretical approach to other more highly charged tungsten ions.

5 Charge Exchange

The discovery of highly charged ions in the solar wind [12, 37] and their interaction with interstellar and planetary atoms, has renewed interest in accurate charge exchange data in the astrophysical community. Predicting charge exchange spectra requires knowledge of state selective $(n\ell)$ charge transfer cross sections. At high collision energies the classical trajectory Monte-Carlo (CTMC) method [72] is quite accurate. At low collision energies the computational challenging atomic-orbital close-coupling (AOCC) method [17, 34] is needed.

A time-dependent lattice (TDL) method was originally developed to study excitation, ionization, and charge transfer in proton collisions with H atoms [32, 33]. The method was then extended to investigate excitation and charge transfer in proton collisions with laser excited Li atom [61, 63]. This same method was also applied to study charge transfer in proton collisions with He atoms [46] and α-particle collisions with H atoms [47].

Recently, charge exchange spectra were measured in C^{6+} collisions with He atoms using a microcalorimeter X-ray detector at the ORNL ion-atom merged-beams facility [14]. Experiments are now in progress to examine charge exchange spectra in C^{6+} collisions with H atoms.

5.1 C^{6+} -H, and He collisions

The time-dependent lattice method is used to calculate state selective charge transfer cross sections in C^{6+} collisions with H and He atoms [62]. The $C^{6+}(n\ell)$ capture cross sections for energies of 2.7, 5.2, and 8.3 keV/amu are found to be in good agreement with recent atomic orbital close-coupling calculations for H and somewhat larger than previous atomic orbital close-coupling calculations for He. Using standard radiative transition rates, Lyman β/α and Lyman γ/α line ratios are calculated using time-dependent lattice and atomic-orbital close-coupling capture cross sections for both H and He. As illustrated in Fig. 7 the theoretical line ratios for He are found to be in suitable agreement with recent experimental measurements [14]. The interested reader should consult the recent work of Pindzola and Fogle [62] for further details.

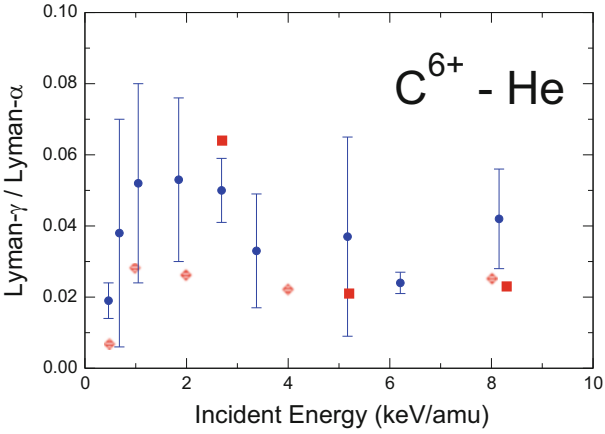

Fig. 7 Lyman-γ/Lyman-α line ratios for C^{6+} -He collisions. *Solid squares* (*red*), time-dependent lattice approach (TDL), *dashed diamonds*, the atomic-orbital close-coupling (AOCC) method [17], and *solid circles* (*blue*) experiment [14]

6 Summary and Future Work

We have vividly illustrated the power of the predictive nature of the R-matrix approach within a non-relativistic or a fully relativistic approach for photoionization cross sections, valence or inner-shell, resonance energy positions, Auger widths and strengths. Access to leadership architectures is essential to our research work such as the Cray XC40 at HLRS which provides an integral contribution to our computational effort.

In future work we intend to extend our R-matrix work to investigate several molecules such as N_2, CO and O_2 for a variety of processes, all of which are of prime interest to aeronomy and astrophysical applications. Furthermore, we draw the reader's attention to our recent work on neutral Sulfur where large-scale DARC cross section calculations were compared to photolysis experiments performed in Berlin [5]. We note that the photolysis experimental work (although contaminated with various molecular precursors) produced rich resonance structures in the experimental spectra that was reproduced well by theory. Large-scale cross sections computations have also been performed for the $2p^{-1}$ removal in Si^+ ions by photons [31]. In addition we have ongoing theoretical efforts dedicated to the modelling of cross sections for $S^+(2s^{-1}$ or $2p^{-1})$ and $SH^+(2\sigma^{-1})$ removal by photons. Finally, recent photoabsorption cross section measurements, for *K*-shell removal, carried out at PETRA III, on N-like neon at the *K*-edge, appears to be reproduced well within an RMPS approach, as is that for B-like carbon, all of which will be reported on in due course in the literature.

Acknowledgements A. Müller and S. Schippers acknowledge support by Deutsche Forschungsgemeinschaft under project numbers M-1068/10 and Mu-1068/20 and through NATO Collabora-

tive Linkage grant 976362. B.M. McLaughlin acknowledges support from the US National Science Foundation through a grant to ITAMP at the Harvard-Smithsonian Center for Astrophysics, under the visitor's program, the RTRA network *Triangle de le Physique* and a visiting research fellowship (VRF) from Queen's University Belfast. C.P. Ballance and M.S. Pindzola acknowledges support by NSF and NASA grants through Auburn University. This research used computational resources at the National Energy Research Scientific Computing Center in Oakland, CA, USA, and at the High Performance Computing Center Stuttgart (HLRS) of the University of Stuttgart, Stuttgart, Germany. The Oak Ridge Leadership Computing Facility at the Oak Ridge National Laboratory, provided additional computational resources, which is supported by the Office of Science of the U.S. Department of Energy under Contract No. DE-AC05-00OR22725. The Advanced Light Source is supported by the Director, Office of Science, Office of Basic Energy Sciences, of the US Department of Energy under Contract No. DE-AC02-05CH11231.

References

1. Al Shorman, M.M., Gharaibeh, M.F., Bizau, J.M., Cubaynes, D., Guilbaud, S., El Hassan, N., Miron, C., Nicolas, C., Robert, E., Sakho, I, Blancard, C., McLaughlin, B.M.: K-Shell Photoionization of Be-like and Li-like Ions of atomic nitrogen: experiment and theory. J. Phys. B At. Mol. Opt. Phys. **46**, 195701 (2013)
2. Ballance, C.P., Griffin D.C.: Relativistic radiatively damped R-matrix calculation of the electron-impact excitation of W^{46+}. J. Phys. B At. Mol. Opt. Phys. **39**, 3617 (2006)
3. Ballance, C.P., McLaughlin, B.M.: Photoionization of the valence shells of the neutral tungsten. J. Phys. B At. Mol. Opt. Phys. **48**, 085201 (2015)
4. Ballance, C.P., Loch S. D., Pindzola M.S., Griffin D.C.: Electron-impact excitation and ionization of W^{3+} for the determination of tungsten influx in a fusion plasma. J. Phys. B At. Mol. Opt. Phys. **46**, 055202 (2013)
5. Barthel, M., Flesch, R., Rühl, E., McLaughlin, B.M.: Photoionization of the $3s^2 3p^4\ ^3$P and the $3s^2 3p^4\ ^1$D,^{1} S states of sulfur: experiment and Theory. Phys. Rev A **91**, 013406 (2015)
6. Bizau, J.M., Esteva, J.-M., Cubaynes, D., Wuilleumier, F.J, Blancard, C., Compant La Fontaine, A., Couillaud, C., Lachkar, J., Marmoret, R., Rémond, C., Bruneau, J., Hitz, D., Ludwig, P., Delaunay, M.: Photoionization of highly charged ions using an ECR ion source and undulator radiation. Phys. Rev. Lett. **84**, 435 (2000)
7. Bizau, J.M., Cubaynes, D., Guilbaud, S., Al Shorman, M.M., Gharaibeh, M.F., Ababneh, I.Q., Blancard, C., McLaughlin, B.M.: K-shell photoionization of O^+ and O^{2+} ions: experiment and theory. Phys. Rev. A **92**, 023401 (2015)
8. Boyle, J., Altun, Z., Kelly H.P.: Photoionization cross-section calculation of atomic tungsten. Phys. Rev. A **47**, 4811 (1993)
9. Chen, M.H., Reed, K.J., McWilliams, D.M., Guo, D.S., Barlow, L., Lee, M., Walker, V.: K-shell Auger and radiative Transitions in the Carbon Isoelectronic Sequence $6 \leq Z \leq 54$. At. Data Nucl. Data Tables **65**, 289 (1997)
10. Costello, J.T., Kennedy, E.T., Sonntag, B.F., Cromer, C.L.: XUV Photoabsorption of laser-generated W and Pt vapours. J. Phys. B At. Mol. Opt. Phys. **24**, 5063 (1991)
11. Covington, A.M., Aguilar, A., Covington, I.R., Hinojosa, G., Shirley, C.A., Phaneuf, R.A., Álvarez, I., Cisneros, C., Dominguez-Lopez, I., Sant'Anna, M. M., Schlachter, A.S., Ballance, C.P., McLaughlin, B.M.: Valence-shell photoionization of chlorine like Ar^+ ions. Phys. Rev. A **84**, 013413 (2011)
12. Cravens, T.E.: Comet Hyakutake X-ray source: Charge transfer of solar wind heavy ions. Geophys. Res. Lett. **24**, 105 (1997)
13. DARC codes http://connorb.freeshell.org

14. Defray, X., Morgan, K., McCammon, D., Wulf, D., Andrianarijaona, V.M., Fogle, M., Seely, D.G., Draganic, I.N., Havener, C.C.: X-ray emission measurements following charge exchange between C^{6+} and He. Phys. Rev. A **88**, 052702 (2013)
15. Dyall, K.G., Grant, I.P., Johnson, C.T., Plummer, E.P.: GRASP: A general-purpose relativistic atomic structure program. Comput. Phys. Commun. **55**, 425 (1989)
16. Fivet, V., Bautista, M.A., Ballance, C.P.: Fine-structure photoionization cross sections of Fe II. J. Phys. B At. Mol. Opt. Phys. **45**, 035201 (2012)
17. Fritsch, W., Lin, C.D.: Atomic-orbital expansion study for the (quasi-)two-electron collision system O^{6+} + He and C^{6+} + He. J. Phys. B At. Mol. Phys. **19**, 2683 (1986)
18. Garcia, J., Mendoza, C., Bautista, M.A., Gorczyca, T.W., Kallman, T.R., Palmeri P.: K-shell photoabsorption of oxygen ions. Astrophys. J. Suppl. Ser. **158**, 68 (2005)
19. Gatuzz, E., Garcia, J. Mendoza, C., Kallman, T.R., Witthoeft, M., Lohfink, A., Bauitista, M.A., Palmeri, P., Quinet, P.: Photoionization modeling of oxygen K absorption in the interstellar medium: The Chandra grating spectra of XTE J1817-330. Astrophys. J. **768**, 60 (2013)
20. Gharaibeh, M.F., Bizau, J.M., Cubaynes, D., Guilbaud, S., El Hassan, N., Al Shorman, M. M., Miron, C., Nicolas, C., Robert, E., Blancard, C., McLaughlin, B.M.: K-shell photoionization of singly ionized atomic nitrogen: experiment and theory. J. Phys. B At. Mol. Opt. Phys. **44**, 175208 (2011)
21. Gharaibeh, M.F., El Hassan, N., Al Shorman, M.M., Bizau, J.M., Cubaynes, D., Guilbaud, S., Blancard, C., McLaughlin, B.M.: K-shell photoionization of B-like atomic nitrogen ions: experiment and theory. J. Phys. B At. Mol. Opt. Phys. **47**, 065201 (2014)
22. Grant, I.P.: Quantum Theory of Atoms and Molecules: Theory and Computation. Springer, New York (2007)
23. Gu, M.F., Schmidt, M., Beiersdorfer, P., Chen, H., Thorn, D.B., Träbert E, Behar, E., Kahn, S.M.: Laboratory measurement and theoretical modeling of K-shell X-ray lines from inner-shell excited and ionized ions of oxygen. Astrophys. J. **627**, 1066 (2005)
24. Haensel, R., Radler, K., Sonntag, B., Kunz, C.: Optical absorption measurements of tantalum, tungsten, rhenium and platinum in the extreme ultraviolet. Solid State Commun. **7**, 1495 (1969)
25. Hasoglu, M.F., Abdel Naby, S.A., Gorczyca, T.W., Drake J.J., McLaughlin, B.M.: K-shell photoabsorption studies of the carbon isonuclear sequence. Astrophys. J. **724**, 1296 (2010)
26. Hinojosa, G., Covington, A.M., Alna'Washi, G.A., Lu, M., Phaneuf, R.A., Sant'Anna, M.M., Cisneros, C., Álvarez, I., Aguilar, A., Kilcoyne, A.L.D., Schlachter, A.S., Ballance, C.P., McLaughlin, B.M.: Valence-shell single photoionization of Kr^{+} ions: experiment and theory. Phys. Rev. A **86**, 063402 (2012)
27. Juett, A.M., Schultz, N.S., Chakrabarty D.: High-resolution x-ray spectroscopy of the interstellar medium structure at the oxygen absorption edge. Astrophys. J. **612**, 308 (2004)
28. Kallman, T.R.: Challenges of plasma modelling: current status and future plans. Space Sci. Rev. **157**, 177 (2010)
29. Kramida, A.E., Ralchenko, Y., Reader, J., NIST ASD Team (2014), NIST Atomic Spectra Database (version 5.2), National Institute of Standards and Technology, Gaithersburg, MD, USA
30. Kawatsura, K., Yamaoka, H., Oura, M., Hayaishi. T., Sekioka, T., Agui, A., Yoshigoe, A., Koike, F.: The $1s-2p$ resonance photoionization measurement of O^{+} ions in comparison with an isoelectronic species Ne^{3+}. J. Phys. B At. Mol. Opt. Phys. **35**, 4147 (2002)
31. Kennedy, E.T., Mosnier, J.-P., Van Kampen, P., Cubaynes, D., Guilbaud, S., Blancard, C., McLaughlin, B.M., Bizau, J.-M.: Photoionization cross sections of the aluminum like Si^{+} ion in the region of the $2p$ threshold (94–137 eV). Phys. Rev. A **90**, 063409 (2014)
32. Kolakowska, A., Pindzola, M.S., Robicheaux, F., Schultz, D.R., Wells, J.C.: Excitation and charge transfer in proton-hydrogen collisions. Phys. Rev. A. **58**, 2872 (1998)
33. Kolakowska, A., Pindzola, M.S., Schultz, D.R.: Total electron loss, charge transfer, and ionization in proton-hydrogen collisions at 10–100 keV. Phys. Rev. A **59**, 3588 (1999)
34. Kimura, M., Olson, R.E.: Electron capture to $(n\ell)$ states in collisions of C^{4+} and C^{6+} with He. J. Phys. B At. Mol. Phys. **17**, L713 (1984)

35. Krantz, C., Spruck, K., Badnell, N.R., Becker, A., Bernhardt, D., Grieser, M., Hahn, M., Novotný, O., Repnow, R., Savin, D.W., Wolf, A., Müller, A., and Schippers S.: Absolute rate coefficients for the recombination of open f-shell tungsten ions. J. Phys. Conf. Ser. **488**, 012051 (2014)
36. Liao, J.-Y., Zhang, S.-N., and Yao, Y.: Wavelength Measurements of K Transitions of Oxygen, Neon, and Magnesium with X-ray Absorption Lines. Astrophys. J. **774** 116 (2013)
37. Lisse, C.M., Dennerl, K., Englhauser, J., Harden, M., Marshall, F.E., Mumma, M.J., Petre, R., Pye, J.P., Ricketts, M.J., Schmitt, J., Trümper J., West, R.G.: Discovery of X-ray and Extreme Ultraviolet Emission from Comet C/Hyakutake 1996 B2. Science **274**, 205 (1996)
38. McLaughlin, B.M.: Inner-shell Photoionization, Fluorescence and Auger Yields. In: Ferland, G., Savin, D.W. (eds.) Spectroscopic Challenges of Photoionized Plasma, Astronomical Society of the Pacific, ASP Con*f*. Series, vol. 247, pp. 87. San Francisco (2001)
39. McLaughlin, B.M., Ballance, C.P.: Photoionization cross section calculations for the halogen-like ions Kr^+ and Xe^+. J. Phys. B At. Mol. Opt. Phys. **45**, 085701 (2012)
40. McLaughlin, B.M., Ballance, C.P.: Photoionization cross-sections for the trans-iron element Se^+ from 18 eV to 31 eV. J. Phys. B At. Mol. Opt. Phys. **45**, 095202 (2012)
41. McLaughlin, B.M., Ballance, C.P.: Photoionization, fluorescence and inner-shell processes. In: McGraw-Hill (eds) McGraw-Hill Yearbook of Science and Technology, pp. 281. Mc Graw Hill, New York (2013)
42. McLaughlin, B.M., Ballance, C.P.:Petascale computations for large-scale atomic and molecular collisions. In: Resch, M.M. Kovalenko, Y., Fotch, E., Bez, W., Kobaysahi, H. (eds.) Sustained Simulated Performance 2014, chap. 15. Springer, New York (2014)
43. McLaughlin, B.M., Bizau, J.M., Cubaynes, D., Al Shorman, M.M., Guilbaud, S., Sakho, I., Blancard, C., Gharaibeh, M.F.: K-shell photoionization of B-like (O^{3+}) oxygen ions: experiment and theory. J. Phys. B At. Mol. Opt. Phys. **47**, 115201 (2014)
44. McLaughlin, B.M., Ballance, C.P., Pindzola, M.S., Müller, A.: PAMOP: petascale atomic, molecular and optical collisions. In: Nagel, W.E., Kröner, D.H., Resch, M.M. (eds.) High Performance Computing in Science and Engineering'14, chap. 4. Springer, New York (2014)
45. McLaughlin, B.M., Ballance, C.P., Bown, K.P., Gardenghi, D.J., Stolte, W.C.: High precision k-shell photoabsorption cross sections for atomic oxygen: experiment and theory. Astrophys, J **771**, L8 (2013) & Astrophys. J 779, L31 (2013)
46. Minami, T., Lee, T.G., Pindzola, M.S.: Coherence parameters for charge transfer in collisions of protons with helium calculated using a hybrid numerical approach. J. Phys. B At. Mol. Opt. Phys. **37**, 4025 (2004)
47. Minami, T., Lee, T.G., Pindzola, M.S., Schultz, D.R.: Total and state-selective charge transfer in He^{2+} + H collisions. J. Phys. B At. Mol. Opt. Phys. **41**, 135201 (2008)
48. Müller, A.: Fusion-related ionization and recombination data for tungsten ions in low to moderately high charge states. Atoms **3**, 120 (2015)
49. Müller, A.: Precision studies of deep-inner-shell photoabsorption by atomic ions. Phys. Scr. **90**, 054004 (2015)
50. Müller, A., Schippers, S., Phaneuf, R.A., Scully, S.W.J., Aguilar, A., Cisneros, C., Gharaibeh, M.F., Schlachter, A.S., McLaughlin, B.M.: K-shell photoionization of Be-like Boron (B^+) Ions: experiment and theory J. Phys. B At. Mol. Opt. Phys. **47**, 135201 (2014)
51. Müller. A., Schippers, S., Kilcoyne, A.L.D., Esteves, D.: Photoionization of tungstens ions with synchrotron radiation. Phys. Scr. **T144**, 014052 (2011)
52. Müller, A., Schippers, S., Kilcoyne, A.L.D., Aguilar, A., Esteves, D., Phaneuf, R.A.: Photoionization of singly and multiply charged tungsten ions. J. Phys. Conf. Ser. **388**, 022037 (2012)
53. Müller, A., Schippers, S., Hellhund, J., Holosto, K., Kilcoyne, A.L.D., Phaneuf, R.A., Ballance, C.P., McLaughlin, B.M.: Single-photon single ionization of W^+ ions: experiment and theory. J. Phys. B At. Mol. Opt. Phys. **48**, 235203 (2015)
54. Müller, A., Schippers, S., Esteves-Macaluso, D., Habibi, M., Aguilar, A., Kilcoyne, A.L.D., Phaneuf, R.A., Ballance, C.P., McLaughlin, B.M.: High resolution valence shell photoionization of Ag-like (Xe^{7+}) Xenon ions: experiment and theory. J. Phys. B At. Mol. Opt. Phys. **4**7, 215202 (2014)

55. Müller, A., Schippers, S., Hellhund, J., Kilcoyne, A.L.D., Phaneuf, R.A., Ballance, C.P., McLaughlin, B.M.: Single and multiple photoionization of W^{q+} tungsten ions in charged states q = 1,2,..,5: experiment and theory J. Phys. Conf. Ser. **488**, 022032 (2014)
56. Neu, R., Dux, R., Geier, A., Gruber, O., Kallenbach, A., Krieger, K., Maier, H., Pugno, R., Rohde, V., Schweizer, S., and ASDEX Upgrade Team: Tungsten as plasma-facing material in ASDEX Upgrade. Fusion Eng. Des. **65**, 367 (2003)
57. Neu, R., Arnoux, G., Beurskens. M., Bobkov, V., Brezinsek, S., Bucalossi, J., Calabro, G., Challis, C., Coenen, J.W., de la Luna, E., de Vries, P.C., Dux, R., Frassinetti. L., Giroud, C., Groth, M., Hobirk, J., Joffrin, E., Lang, P., Lehnen, M., Lerche, E., Loarer, T., Lomas, P., Maddison, G., Maggi, C., Matthews, G., Marsen, S., Mayoral, M.L., Meigs, A., Mertens, P., Nunes, I., Philipps, V., Pütterich, T., Rimini, F., Sertoli, M., Sieglin, B., Sips, A.C.C., van Eester, D., van Rooij, G., JET-EFDA Contributors: First operation with the JET International thermonuclear reactor-like Wall. Phys. Plasmas **20**, 056111 (2013)
58. Norrington, P.H., Grant, I.P: Low-energy electron scattering by Fe XXIII and Fe VII using the Dirac R-matrix method. J. Phys. B At. Mol. Opt. Phys. **20**, 4869 (1987)
59. Olalla, E., Wilson, N.J., Bell, K.L., Martin, I., Hibbert, A.: Inner-shell photoionization of O III. Mon. Not. R. Astron. Soc. **332**, 1005 (2002)
60. Parpia, F., Froese-Fischer, C., Grant, I.P.: GRASP92: a package for large-scale relativistic atomic structure calculations. Comput. Phys. Commun. **94**, 249 (2006)
61. Pindzola, M.S.: Proton-impact excitation of laser-excited lithium atoms. Phys. Rev. A **66**, 032716 (2002)
62. Pindzola, M.S., Fogle, M.: Single charge transfer in C^{6+} collisions with H, He atoms. J. Phys. B At. Mol. Opt. Phys. **48**, 205203 (2015)
63. Pindzola, M.S., Minami, T., Schultz, D.R.: Laser-modified charge-transfer processes in proton collisions with lithium atoms. Phys. Rev A **68**, 013404 (2003)
64. Petrini, D., da Silva, E.P.: Soft X irradiation of low density plasmas: O III and O IV line emission. Rev. Mex. Astron. Astrofis. **32**, 69 (1996)
65. Pradhan, A.K., Chen, G.X., Delahaye, F., Nahar, S.N., Oelgoetz, J.: X-ray absorption via K_α resonance complexes in oxygen ions. Mon. Not. R. Astron. Soc. **341**, 1268 (2003)
66. Rausch, J., Becker, A., Spruck, K., Hellhund, J., Borovik Jr, A., Huber, K., Schippers S., and Müller, A.: Electron-impact single and double ionization of W^{17+}. J. Phys. B At. Mol. Opt. Phys. **44**, 165202 (2011)
67. Sant'Anna, M.M., Schlachter, A.S., Öhrwall, G., Stolte, W.C., Lindle, D.W., McLaughlin, B.M.: K-shell X-ray spectroscopy of atomic nitrogen. Phys. Rev. Lett. **107**, 033001 (2011)
68. Sala, G., Greiner, J., Bottacini, E., Haberl, F.: XMM-Newton and INTEGRAL observations of the black hole candidate XTE J1817-330. Astrophys. Space Sci. **309**, 315 (2007)
69. Saloman, E.B.: Energy levels and observed spectral lines of Xenon, Xe I through Xe LIV. J. Phys. Chem. Ref. Data **33**, 765 (2004)
70. Schippers, S., Muller, A., Esteves, D., Habibi, M., Aguilar, A., Kilcoyne, A.L.D.: Experimental absolute cross section for photoionization of Xe^{7+}. J. Phys. Conf. Ser. **194**, 022094 (2009)
71. Schippers, S., Bernhardt, D., Müller, A., Krantz, C., Grieser, M., Repnow, R., Wolf, A., Lestinsky, M., Hahn, M., Novotný, O. Savin, D.W.: Dielectronic recombination of xenon like tungsten ions. Phys. Rev. A **83**, 012711 (2011)
72. Simcic, J., Schultz, D.R., Mawhorter, R.J., Cadez, I., Greenwood, J.B., Chutjian, A., Liesse, C.M., Smith, S.J.: Measurement and calculation of absolute single-and multiple-charge-exchange cross sections for Fe^{q+} ions impacting CO and CO_2. Phys. Rev. A **81**, 062715 (2010)
73. Sladeczek, P., Feist, H., Feldt, M., Martins, M., Zimmermann, P.: Photoionization Experiments with an Atomic Beam of Tungsten in the Region of the $5p$ and $4f$ excitation. Phys. Rev. Lett. **75**, 1483 (1995)
74. Spruck, K., Badnell, N.R., Krantz, C., Novotný, O., Becker, A., Bernhardt, D., Grieser, M., Hahn, M., Repnow, R., Savin, D.W., Wolf, A., Müller, A., Schippers S.: Recombination of W^{18+} ions with electrons: absolute rate coefficients from a storage-ring experiment and from theoretical calculations. Phys. Rev. A **90**, 032715 (2014)

75. Stenke, M., Aichele, K., Harthiramani, D., Hofmann, G., Steidl, M., Völpel, R., and Salzborn E.: Electron-impact single-ionization of singly and multiply charged tungsten ions. J. Phys. B At. Mol. Opt. Phys. **28**, 2711 (1995)
76. Trzhaskovskaya, M.B., Nikulin, V.K., Clark, R.E.H.: Radiative recombination rate coefficients for highly-charged tungstens ions. At. Data Nucl. Data Tables **96**, 1 (2010)
77. Wijesundera, W.P., Parpia, F.A., Grant, I.P., Norrington, P.H.: Electron scattering by Kr XXIX (oxygen-like krypton) using the Dirace R-matrix method. J. Phys. B At. Mol. Opt. Phys. **24** 1803 (1991)
78. Yao, Y., Schultz, N.S., Gu, M.F., Nowak, M.A., and Cainizares, C.: High-resolution X-ray spectroscopy of the multiphase interstellar medium towards Cyg X-2. Astrophys. J. **696** 1418 (2009)
79. Zeng, J., Zhao,G., Yuan, J.: The $1s \rightarrow 2p$ resonance photoionization from the low-lying states of O^+ - Energies, autoionization widths, branching ratios, and oscillator strengths. Eur. Phys. J. D **28**, 163 (2004)
80. Zeng, J., Yuan, J., Lu, Q.: Photoionization of O III low-lying states: autoionization resonances energies and widths of some $1s - 2p$ excited states. J. Phys. B. At. Mol. Opt. Phys. **34**, 2823 (2001)